Oscillation with Photorefractive Gain

SZE-KEUNG KWONG, MARK CRONIN-GOLOMB, AND AMNON YARIV, FELLOW, IEEE

Abstract—**We review theories and experimental demonstrations of oscillation with photorefractive gain. The unidirectional ring resonator, the linear passive phase conjugate mirror, a phase conjugate resonator (the semilinear passive phase conjugate mirror), and the double phase conjugate resonator are treated, the applications in path-length-to-frequency converting interferometers and one-way wavefront converters are described.**

ONE recent development in the field of phase conjugate optics has been the demonstration of oscillation in photorefractively pumped oscillators and new devices and phenomena which are related to it. This paper will review all of these developments, starting with photorefractive gain based on two-beam coupling in Section I. We then apply the theory to a ring resonator in Section I-A. In Section I-B, the theoretical treatment is extended beyond the plane wave case to an interference pattern which produces a complicated hologram, rather than a simple grating. In Section II, we shall discuss photorefractive pumped oscillation based on four-wave mixing, and some specific examples will be discussed: a) linear resonator (with two conventional mirrors); b) phase conjugate resonator (with one conventional resonator and one phase conjugate mirror); and c) double phase conjugate resonator. In Section III, we shall discuss two applications of the above anaysis a) optical-path-length-to-frequency conversion interferometer and b) one-way real-time wavefront converters.

I. Two-Beam Coupling Theory

We start by reviewing the interaction between two coherent beams interfering inside a photorefractive crystal (Fig. 1) [1], [2]. The intensity variation of the interference pattern causes the charge carriers inside the crystal to redistribute themselves by drift and diffusion. Then the electric field associated with the space charge operates through the electrooptic effect to produce a refractive index grating. In general, there is a spatial phase shift between the light interference pattern and the index grating. This phase shift introduces an asymmetry that allows one beam to be amplified by constructive interference with radiation scattered by the grating, while the other beam is attenuated by destructive interference with diffracted radiation [3], [4]. This asymmetry is available because we are using the linear electrooptic effect, which is not invariant under space inversion and can only arise in noncentrosymmetric media. In addition, the phase delays after passing through the interaction region for each beam may be affected by the nonlinear interaction [5], [6]. Both the energy coupling and the phase delay are important in analyzing the oscillation condition of a resonator.

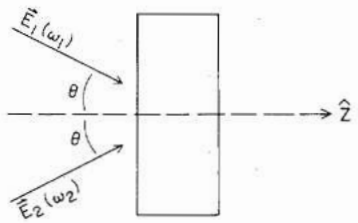

Fig. 1. A schematic diagram of two-beam coupling.

Referring to the configuration shown in Fig. 1, we assume that both beam 1 and beam 2 are plane waves and can be written as

$$\boldsymbol{E}_j = \boldsymbol{A}_j(\boldsymbol{r}) \exp\left[i(\boldsymbol{k}_j \cdot \boldsymbol{r} - \omega_j t)\right] + \text{c.c.} \qquad j = 1, 2. \tag{1}$$

Using the scalar wave equation and the standard slowly varying field approximation, we can obtain the following coupled wave equations [7]:

$$\frac{dI_1}{ds} = -\Gamma \frac{I_1 I_2}{I_0} - \alpha I_1 \tag{2a}$$

$$\frac{dI_2}{ds} = \Gamma \frac{I_1 I_2}{I_0} - \alpha I_2 \tag{2b}$$

$$\frac{d\psi_1}{ds} = -\Gamma' \frac{I_2}{I_0} \tag{2c}$$

$$\frac{d\psi_2}{ds} = -\Gamma' \frac{I_1}{I_0} \tag{2d}$$

where

$$s = z/\cos\theta$$

$$I_j = |A_j|^2 \quad \text{and} \quad A_j = |A_j| \exp[i\psi_j] \qquad j = 1, 2 \tag{3}$$

$$I_0 = I_1 + I_2$$

$$\Gamma = 2 \operatorname{Re}[\gamma], \qquad \Gamma' = \operatorname{Im}[\gamma], \tag{4}$$

and from standard photorefractive theory, the (complex)

Manuscript received December 30, 1985. This work was supported in part by the U.S. Air Force Office of Scientific Research and in part by the U.S. Army Research Office.

S.-K. Kwong and M. Cronin-Golomb are with Ortel Corporation, Alhambra, CA 91803.

A. Yariv is with the California Institute of Technology, Pasadena, CA 91125.

IEEE Log Number 8608675.

0018-9197/86/0800-1508$01.00 © 1986 IEEE

coupling constant γ is given by [8], [9]

$$\gamma = \frac{\omega r_{\text{eff}} n_0^3}{4c} \frac{E_q(E_0 + iE_D)}{[E_0 - (\omega_2 - \omega_1)\, t_0(E_D + E_\mu)] + i[E_D + E_q + (\omega_2 - \omega_1)t_0E_0]} \tag{5}$$

where θ is the angle between the beams and the z-axis, α is the intensity absorption coefficient, r_{eff} is the relevant electrooptic coefficient, n_o is the ordinary refractive index of the crystal, $t_0 = N_A/\alpha N I_0$ is the characteristic time, N_A is the concentration of trapping centers, E_0 is the externally applied dc electric field, E_μ, E_D, and E_q are internal electric fields characteristic of drift, diffusion, and maximum space charge, respectively. The parameters r_{eff}, t_0, E_μ, E_D, and E_q can be calculated from crystal properties and crystal orientation with respect to the various interacting beams. Since, as we will show in what follows, $(\omega_2 - \omega_1)/\omega_1 < 10^{-14}$, ω_1 and ω_2 can be accurately replaced by $\omega_2 \simeq \omega_1$ except in (5) so that the magnitudes of coupling strengths Γ and Γ' are the same for $\boldsymbol{E}_1$ and $\boldsymbol{E}_2$. This approximation will be justified later.

When there is no applied electric field, $E_0 = 0$,

$$\gamma = \frac{\gamma_0}{1 + i(\omega_2 - \omega_1)\tau} \tag{6}$$

where

$$\gamma_0 = \frac{\omega r_{\text{eff}} n_0^3}{4c} \frac{E_q E_D}{(E_q + E_D)} \tag{7}$$

and

$$\tau = t_0 \left[\frac{E_D + E_\mu}{E_D + E_q}\right]. \tag{8}$$

From (2) we note that the intensity coupling is due to the real part of the coupling constant γ and the phase delay is due to the imaginary part of γ. Equation (2) can be solved with the boundary conditions $|A_j(0)|\exp[i\psi_j(0)]$, $j = 1, 2$,

$$I_1(s) = \frac{I_0(0)\, e^{-\alpha s}}{1 + (I_2(0)/I_1(0))\, e^{\Gamma s}}$$

$$I_2(s) = \frac{I_0(0)\, e^{-\alpha s}}{1 + (I_1(0)/I_2(0))\, e^{-\Gamma s}}$$

$$\psi_1(s) = \psi_1(0) - \Gamma' s + \frac{\Gamma'}{\Gamma} \ln\left[\frac{1 + I_1(0)/I_2(0)}{1 + (I_1(0)/I_2(0))\, e^{\Gamma s}}\right] \tag{9c}$$

$$\psi_2(s) = \psi_2(0) - \Gamma' s - \frac{\Gamma'}{\Gamma} \ln\left[\frac{1 + I_2(0)/I_2(0)}{1 + (I_2(0)/I_1(0))\, e^{\Gamma s}}\right]. \tag{9d}$$

Equations (9a) and (9b) describe coherent optical gain for beam 2 and loss for beam 1, and (9c) and (9d) describe the phase transfer between beam 1 and beam 2.

Unlike gain from population inversion, spontaneous emission is not an important source of noise in photorefractive gain. However, noise does arise from scattering imperfections in the crystal and random thermal excitation of carriers into the conduction band (as opposed to deliberate photoexcitation).

A. Ring Resonator

The simplest oscillator utilizing photorefractive gain is the ring oscillator, which is shown in Fig. 2. The pumping beam I_1 provides photorefractive gain for the oscillation beam I_2 going in one direction; therefore, this is a "unidirectional" ring oscillator [4], [5], [10]–[13]. Since only two-beam coupling is involved, we can apply the theory developed in the above section.

We apply boundary conditions appropriate to a ring oscillator,

$$I_2(0) = RI_2(l), \tag{10}$$

where l is the interaction length and R is the combined reflectivity for one roundtrip. From (9) and (10), we can solve for $I_2(0)$ and $[\psi_2(l) - \psi_2(0)]$:

$$I_2(0) = I_1(0)\left[\frac{1 - e^{-\Gamma l}}{1 - R\, e^{-\alpha l}} - 1\right] \tag{11}$$

$$\psi_2(l) - \psi_2(0) = -\frac{\Gamma'}{\Gamma}(\alpha l - \ln R). \tag{12}$$

Equation (11) gives the intensity of oscillation and (12) gives the phase shift of A_2 due to the nonlinear interaction. The oscillation conditions are that the roundtrip beam amplitude returns to its original value and the round phase delay is some multiple of 2π. From (11), the roundtrip amplitude condition is

$$\Gamma l > (\Gamma l)_{th} = \alpha l - \ln R. \tag{13}$$

From (4) and (6), we rewrite (12) as

$$\psi_2(l) - \psi_2(0) = \tfrac{1}{2}(\omega_2 - \omega_1)\, \tau(\alpha l - \ln R). \tag{14}$$

The roundtrip phase condition for mode a is

$$\frac{\omega_a L}{c} = \frac{\omega L}{c} + \psi_2(l) - \psi_2(0) \tag{15}$$

where ω_a is the ath mode frequency of the resonator with no photorefractive interaction and L is the length of the resonator. We substitute (14) into (15) and we get

$$(\omega_2 - \omega_1) = \frac{2L}{c(\alpha l - \ln R)\tau}(\omega_a - \omega_2) = \frac{\omega_a - \omega_1}{1 + \dfrac{\tau}{2t_a}} \tag{16}$$

where t_a is the decay time constant of the photon density in the ath mode. In the limit $t_a \lll \tau$, we can approxi-

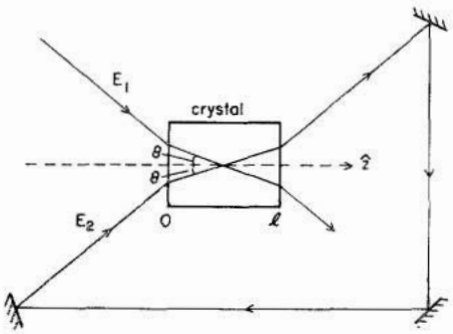

Fig. 2. A schematic diagram of photorefractively pumped unidirectional ring oscillator.

mate (16) by

$$(\omega_2 - \omega_1) \simeq \frac{2t_a}{\tau}(\omega_a - \omega_1). \tag{17}$$

Since for most photorefractive crystals, τ is on the order of 1 s at the intensities commonly used and $t_a(\omega_a - \omega_1)$ is roughly equal to one, $\omega_2 - \omega_1$ is on the order of a few hertz. Therefore, the approximation in (2), $\omega_2 = \omega_1$, is well justified. Equation (17) determines the oscillation frequency. If we choose the zero detuning $\omega_a - \omega_1 = 0$ as the origin, we can rewrite the frequency detuning $\delta = (\omega_2 - \omega_1)$ in (17) as

$$\delta = \frac{2t_a}{\tau}\frac{\omega_1}{L}\Delta L \qquad \left(-\frac{\lambda}{2} \le \Delta L \le \frac{\lambda}{2}\right) \tag{18}$$

where ΔL is the change in cavity length from the origin. We recall that τ, from (8), is inversely proportional to the sum of the pumping and oscillation beam intensities. From (8), (11), and (17),

$$\tau(s, \Delta L) = \left[\frac{E_D + E_\mu}{E_D + E_q}\right]\frac{N_A}{\alpha N}\left[I_1(0)\, e^{-\alpha s}\,\frac{1 - \exp\left(-\frac{\omega_1}{c}\,\frac{2\gamma_0 l}{1 + 4t_a^2\omega_1^2(\Delta L)^2/L^2}\right)}{1 - R\, e^{-\alpha l}}\right]^{-1}. \tag{19}$$

Combining (18) and (19), we can obtain a relationship between the frequency detuning δ and the mirror displacement ΔL. Assuming no absorption, theoretical plots of frequency detuning and the oscillation intensity versus mirror displacement are shown in Fig. 3(a) and (b), respectively.

The theory presented above has been tested experimentally [4], [12] using the apparatus shown in Fig. 4. The output from a single-longitudinal-mode argon ion laser ($\lambda = 514.5$ nm, $P = 0.2$ W, beam diameter = 2 mm) was directed to a poled $BaTiO_3$ crystal. The crystal c-axis was in the plane of the ring oscillator to make use of the large electrooptic coefficient r_{42}. Mirrors M_1, M_2, and M_3 were aligned to form a ring resonator ($L = 38$ cm). Mirror M_1 was set on a piezoelectric mount. A 0.6 mm diameter pinhole was inserted inside the oscillating cavity in order to force a stable single-transverse-mode oscillation (without the pinhole, the oscillation pattern varied erratically in time) [14]. A fraction of the oscillating beam reflected

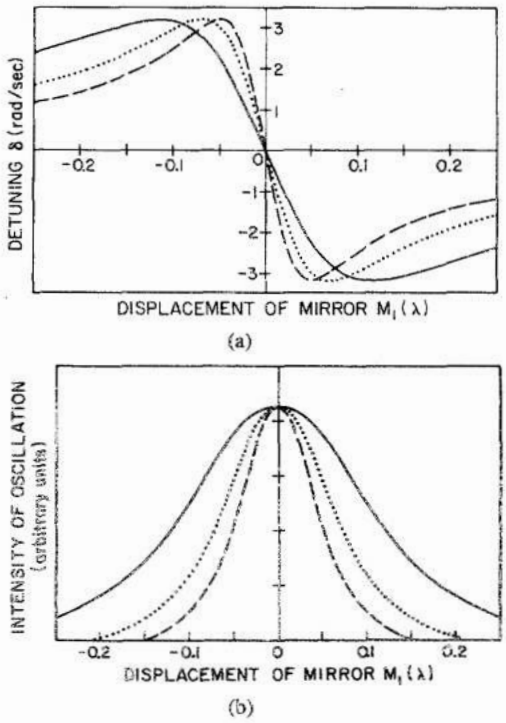

Fig. 3. Theoretical plots. (a) Frequency detuning. (b) Oscillation intensity versus mirror displacement in a ring resonator. $\gamma_0 l = -1.5$, $R = 0.9$ and $4\pi t_a c/L = 15$(——), 25(· · ·), and 35(- - -).

from the front surface of the crystal was combined with the pumping laser beam to form interference fringes. Detector D_1 monitored the speed of moving fringes, from which the frequency offset δ was inferred.

Fig. 5 shows the experimental result of frequency detuning δ against the displacement of mirror M_1, which agrees qualitatively with Fig. 3. The gain linewidth is, according to (6), τ^{-1} Hz, which in $BaTiO_3$ is a few hertz, so that the maximum detuning δ observed is a few hertz. We notice that the oscillator can support two transverse modes, TEM_{00} and TEM_{01}. From Fig 5(a), the slopes of frequency detuning versus the mirror displacement curves give, according to (18), an estimate of the ratio t_a/τ which is 1.89×10^{-8} and 0.88×10^{-8} for the TEM_{00} and the TEM_{01} modes, respectively. This ratio t_a/τ is larger for the TEM_{00} mode than the TEM_{01} mode since the latter, suffering higher diffraction losses, has a smaller t_a. At each region of discontinuity in δ, for example at 0.18λ, 0.6λ, 1.1λ, and 1.65λ, the oscillation was unstable, and rapid mode hopping between the TEM_{00} and TEM_{01} modes was observed. At other points, transitions between TEM_{00} and TEM_{01} could be induced by disturbing the system, for example, by vibrating one of the ring cavity mirrors. The longitudinal mode spacing was 7.9×10^8

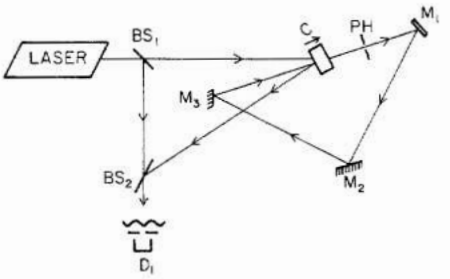

Fig. 4. Experimental configuration for measuring frequency detuning δ versus displacement of mirror M_1. Using a Cartesian coordinate system with the laser beam traveling along the abscissa and the coordinate in inches, the elements are the Ar laser (0, 0); beam splitters BS_1 (1, 0), BS_2 (1, −3.5); mirrors M_1 (9, 1), M_2 (7, −3), and M_3 (3, −1); crystal C (6, 0); 0.6 mm diameter pinhole PH (7.5, 0.5); and detector D_1 (1, −4.5).

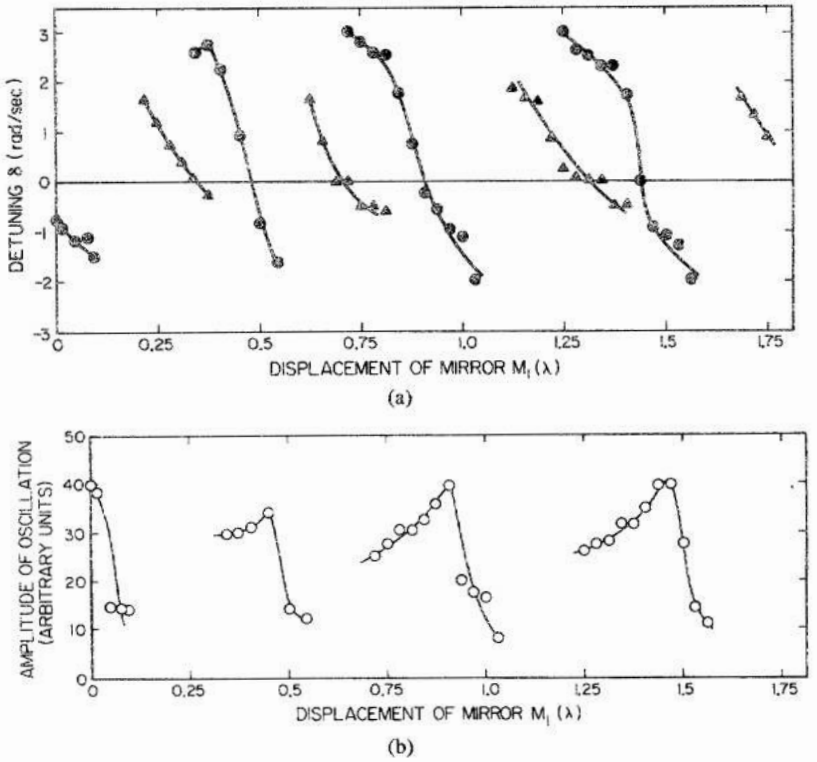

Fig. 5. (a) Experimental data of frequency detuning δ versus displacement of mirror M_1, TEM_{00} mode (•), TEM_{01} mode (Δ). (b) The oscillating beam power of TEM_{00} mode versus displacement of mirror M_1.

Hz, and the transverse mode spacing between TEM_{00} and TEM_{01} modes was 2.13×10^8 Hz. The power of the oscillating beam for the TEM_{00} mode was also plotted in Fig. 5(b). The oscillation power was near maximum at zero frequency detuning, $\delta = 0$, which is due to the fact that at this point the coupling constant γ as given by (6) is maximum.

By using an additional pumping beam to pump the oscillation in the opposite direction, bidirectional oscillation in a ring resonator was experimentally observed by White *et al.* [10] and Rajbenbach *et al.* [13]. A theoretical analysis of photorefractive coupling of counterpropagating traveling waves in ring resonators has been reported by Yeh [15]. The inequality in transmittivities and phase shifts leads to a splitting in both oscillation frequency and intensity.

B. General Oscillator Theory

Here we develop a theory for oscillation in an optical resonator with photorefractive gain. We use an approach similar to Lamb's self-consistent analysis of an inhomogeneous laser [16], [17]. Referring to Fig. 2, we take the known input (pump) beam as

$$E_1(r, t) = \tfrac{1}{2} E_{10}(r)\, e^{j\omega_1 t} + \text{c.c.} \tag{20}$$

where $E_{10}(r)$ contains the propagation factor as well as describing the effect of distortion and of information (spatial) modulation of the beam. The oscillation beam which establishes itself in the ring oscillator is taken as $E_2(r, t)$, and our immediate task is to solve for the oscillation condition and the oscillation frequency of this beam. The resonator field can be expanded in the (complete) set of res-

onator modes $\boldsymbol{E}_a(\boldsymbol{r})$ [18]:

$$\boldsymbol{E}_2(\boldsymbol{r}, t) = \sum_a -\frac{1}{\sqrt{\epsilon}} p_a(t)\, \boldsymbol{E}_a(\boldsymbol{r}) \tag{21a}$$

$$\boldsymbol{H}_2(\boldsymbol{r}, t) = \sum_a \frac{1}{\sqrt{\mu}} \omega_a q_a(t)\, \boldsymbol{H}_a(\boldsymbol{r}) \tag{21b}$$

where

$$\nabla \times \boldsymbol{E}_a = k_a \boldsymbol{H}_a \tag{22a}$$

$$\nabla \times \boldsymbol{H}_a = k_a \boldsymbol{E}_a \tag{22b}$$

$$\omega_a = k_a(\mu\epsilon)^{-1/2}. \tag{22c}$$

$\boldsymbol{E}_a(\boldsymbol{r})$ and $\boldsymbol{H}_a(\boldsymbol{r})$ satisfy the resonator boundary conditions for electric and magnetic fields, respectively. $\epsilon(\boldsymbol{r})$ and μ are electric and magnetic permittivities, respectively. ω_a and k_a are the radian oscillation frequency and wavenumber of the ath mode, respectively. The quantities $p_a(t)$ and $q_a(t)$ contain the temporal information of mode a, including that of the frequency. In addition, the modal functions $\boldsymbol{E}_a$ and $\boldsymbol{H}_a$ are orthonormal according to

$$\int_{V_{\text{res}}} \boldsymbol{E}_a \cdot \boldsymbol{E}_b\, dV = \delta_{ab}$$

and

$$\int_{V_{\text{res}}} \boldsymbol{H}_a \cdot \boldsymbol{H}_b\, dV = \delta_{ab}. \tag{23}$$

The resonator contains a distributed polarization field $\boldsymbol{P}_{\text{NL}}(\boldsymbol{r}, t)$ due to the nonlinear interaction, so that Maxwell's equations can be written as

$$\nabla \times \boldsymbol{H} = \boldsymbol{i} + \frac{\partial}{\partial t}(\epsilon_0 \boldsymbol{E} + \boldsymbol{P}_{\text{nonresonant}} + \boldsymbol{P}_{\text{NL}})$$

$$= \sigma(\boldsymbol{r})\boldsymbol{E} + \epsilon(\boldsymbol{r}) \frac{\partial \boldsymbol{E}}{\partial t} + \frac{\partial}{\partial t} \boldsymbol{P}_{\text{NL}} \tag{24a}$$

$$\nabla \times \boldsymbol{E} = -\mu \frac{\partial \boldsymbol{H}}{\partial t} \tag{24b}$$

where $\sigma(\boldsymbol{r})$ is the effective conductivity that is introduced to account for the losses. Using (21), (22), and (24), the resonator field will satisfy the equation

$$\sum_a \frac{1}{\sqrt{\mu}} \omega_a q_a k_a \boldsymbol{E}_a = -\sigma \sum_a \frac{1}{\sqrt{\epsilon}} p_a \boldsymbol{E}_a - \sum_a \sqrt{\epsilon}\, \dot{p}_a \boldsymbol{E}_a + \frac{\partial}{\partial t} \boldsymbol{P}_{\text{NL}}(\boldsymbol{r}, t) \tag{25}$$

Dot multiplying (25) by $\boldsymbol{E}_b$, integrating over the resonator volume V_{res}, and using the orthonormality condition (22) leads to

$$\omega_b^2 q_b + \frac{\sigma}{\epsilon} p_b + \dot{p}_b - \frac{1}{\sqrt{\epsilon}} \frac{\partial}{\partial t} \int_V \boldsymbol{P}_{\text{NL}} \cdot \boldsymbol{E}_b\, dv = 0$$

$$\omega_b^2 \dot{q}_b + \frac{\sigma}{\epsilon} \dot{p}_b + \ddot{p}_b - \frac{1}{\sqrt{\epsilon}} \frac{\partial^2}{\partial t^2} \int_V \boldsymbol{P}_{\text{NL}} \cdot \boldsymbol{E}_b\, dv = 0. \tag{26}$$

Substituting (21a) into (24b) and using (21b), we obtain

$$p_b = \dot{q}_b, \tag{27}$$

so that (26) becomes (without loss of generality, we use subscript a to represent the oscillating mode)

$$\ddot{p}_a + \frac{\omega_a}{Q_a} \dot{p}_a + \omega_a^2 p_a = \frac{1}{\sqrt{\epsilon}} \frac{\partial^2}{\partial t^2} \int_{V_{\text{res}}} \boldsymbol{P}_{\text{NL}}(\boldsymbol{r}, t) \cdot \boldsymbol{E}_a(\boldsymbol{r})\, dV \tag{28}$$

where $Q_a = \omega_a \epsilon/\sigma$ is the quality factor of the resonator for mode a and $\boldsymbol{P}_{\text{NL}}(\boldsymbol{r}, t)$ is the polarization in the photorefractive crystal due to the nonlinear interaction between the pump (input) beam $\boldsymbol{E}_1(\boldsymbol{r}, t)$ and the oscillator field $\boldsymbol{E}_2(\boldsymbol{r}, t)$. From (26) we identify ω_a as the resonance frequency of mode a in the no loss ($Q_a \to \infty$) limit. The distributed nonlinear polarization term $\boldsymbol{P}_{\text{NL}}(\boldsymbol{r}, t)$ driving the oscillation of the resonator field is that produced by the incidence of the input field $\boldsymbol{E}_1(\boldsymbol{r}, t)$ on the index grating created photorefractively by the interaction of the field $\boldsymbol{E}_1(\boldsymbol{r}, t)$ and the ring oscillator field $\boldsymbol{E}_2(\boldsymbol{r}, t)$. If we assume that one mode only, say a, oscillates, then we may replace $\boldsymbol{E}(\boldsymbol{r}, t)$ by the ath summand in (21) and write

$$\boldsymbol{P}_{\text{NL}}(\boldsymbol{r}, t) = \text{Re}\,[\epsilon_0 \Delta n(\boldsymbol{r}, t)\, \boldsymbol{E}_1(\boldsymbol{r}, t)] \tag{29}$$

where Δn, the index grating formed by the interference of the input beam $\boldsymbol{E}_{10}(\boldsymbol{r})\, e^{i\omega_1 t}$ and the oscillation field $\epsilon^{-1/2} p_a(t)\, \boldsymbol{E}_a(\boldsymbol{r})$ is given by [19]

$$\Delta n(\boldsymbol{r}, t) = -\frac{2ci\gamma}{\omega_2 \sqrt{\epsilon}} \frac{p_{a0}(t)[\boldsymbol{E}_{10}^* \cdot \boldsymbol{E}_a]\, e^{-i(\omega_2 - \omega_1)t}}{|\boldsymbol{E}_{10}|^2 + \frac{1}{\epsilon} |p_a \boldsymbol{E}_a|^2} + \text{c.c.} \tag{30}$$

and then

$$\boldsymbol{P}_{\text{NL}}(\boldsymbol{r}, t) = -\frac{2\epsilon_0 c}{\omega_2 \sqrt{\epsilon}} i\gamma \frac{p_{a0}(t)[\boldsymbol{E}_{10}^* \cdot \boldsymbol{E}_a]\, \boldsymbol{E}_{10}\, e^{i\omega_2 t}}{|\boldsymbol{E}_{10}|^2 + \frac{1}{\epsilon} |p_a \boldsymbol{E}_a|^2} + \text{c.c.} \tag{31}$$

where we take $p_a(t)$ as the product of a slowly varying amplitude $p_{a0}(t)$ and an optical oscillation term exp ($i\omega t$)

$$p_a(t) = p_{a0}(t)\, e^{i\omega_2 t} \tag{32}$$

where γ is given in (5). We note that the sole time dependence of $\boldsymbol{P}_{\text{NL}}(\boldsymbol{r}, t)$ is that of mode a, i.e., of the term $p_a(t)$. The time dependence of the input mode $\boldsymbol{E}_1(\boldsymbol{r}, t)$ has disappeared since $\boldsymbol{E}_1$ appears in (31) multiplied by its complex conjugate. Another, equivalent way to explain this fact is that the index grating produced by the interference of $\boldsymbol{E}_1$ and $\boldsymbol{E}_a$ (the cavity field) is moving since $\omega_2 \neq \omega_1$, and this velocity is just the right one to Doppler shift the incident frequency ω_1 to ω_2.

The oscillator equation (28) becomes

$$\left[(\omega_a^2 - \omega_2^2) + i\frac{\omega_a\omega_2}{Q_a}\right] p_{a0}(t) + \left(2i\omega_2 + \frac{\omega_a}{Q_a}\right) \cdot \dot{p}_{a0} + \ddot{p}_{a0}\, e^{i\omega_2 t} = -\frac{2\epsilon_0 ci\gamma}{\omega_2\epsilon}\frac{\partial^2}{\partial t^2} \cdot \int_{V_{\text{crystal}}} \frac{P_{a0}(t)\,|\boldsymbol{E}_{10}^* \cdot \boldsymbol{E}_a|^2}{|\boldsymbol{E}_{10}|^2 + \frac{1}{\epsilon}\,|p_{a0}(t)\,\boldsymbol{E}_a(\boldsymbol{r})|^2}\, e^{i\omega_2 t}\, dv. \quad (33)$$

As steady state $\dot{p}_a$, $\ddot{p}_a$ vanish, $\partial/\partial t \to i\omega_2$, and $p_{a0}(t) = p_{a0}(\infty) =$ constant. The oscillation condition (33) becomes

$$(\omega_a^2 - \omega_2^2) + i\frac{\omega_a\omega_2}{Q_a} = \frac{2\epsilon_0\omega_2 c}{\epsilon} i\gamma f = i\frac{2\epsilon_0\omega_2 c}{\epsilon}\,\mathrm{f}\,\frac{\gamma_0}{1 + i(\omega_2 - \omega_1)\tau} \quad (34)$$

where in the second equality we used the zero external field ($E_0 = 0$) form of κ as given by (6), and f is given by

$$f = \int_{V_{\text{crystal}}} \frac{|\boldsymbol{E}_{10}^*(\boldsymbol{r}) \cdot \boldsymbol{E}_a(\boldsymbol{r})|^2\, dv}{|\boldsymbol{E}_{10}(\boldsymbol{r})|^2 + \frac{1}{\epsilon}\,|p_{a0}(\infty)\,\boldsymbol{E}_a(\boldsymbol{r})|^2} \quad (35)$$

so that it is dimensionless and real.

The left-hand side of (34) is a complex number which depends only on passive resonator parameters and the (yet unknown) oscillation frequency ω_1. According to (31), the phase of the right-hand side of (31) depends on $(\omega_2 - \omega_1)$. The frequency ω_1 will thus adjust itself relative to ω_2 so as to satisfy (34); using (31) and separating the real and imaginary parts of (34) leads to

$$\omega_a^2 - \omega_2^2 = \frac{2c\epsilon_0 f\gamma_0\omega_2(\omega_2 - \omega_1)\tau}{\epsilon[1 + (\omega_2 - \omega_1)^2\tau^2]} \quad (36)$$

and

$$\frac{\omega_a\omega_2}{Q_a} = \frac{2c\epsilon_0 f\gamma_0\omega_2}{\epsilon[1 + (\omega_2 - \omega_1)^2\tau^2]}, \quad (37)$$

and since $\omega_1 \simeq \omega_a$, (36) and (37) can be accurately approximated by

$$\omega_a - \omega_2 = \frac{2\epsilon_0 f\gamma_0(\omega_2 - \omega_1)\tau}{2\epsilon[1 + (\omega_2 - \omega_1)^2\tau^2]}. \quad (38)$$

In the limit $t_a \lll \tau$ where $t_a = Q_a/\omega_a$ is the decay time constant of the photon density in the ath mode (with no photorefractive interaction) we can solve (38) for ω and, using (37), obtain

$$(\omega_2 - \omega_1) \simeq 2\frac{t_a}{\tau}(\omega_a - \omega_1), \quad (39)$$

which agrees exactly with the two-beam coupling theory analysis (17).

Let us return next to the threshold condition (37). The parameter f is given by (35) and can be written as

$$f = \int \frac{|\boldsymbol{E}_{10}^*(\boldsymbol{r}) \cdot \boldsymbol{E}_a(\boldsymbol{r})|^2}{|\boldsymbol{E}_{10}(\boldsymbol{r})|^2 + |\boldsymbol{E}_{\text{osc}}(\boldsymbol{r})|^2}\, dv \quad (40)$$

$$\simeq \frac{1}{1 + \frac{\langle|\boldsymbol{E}_{\text{osc}}|^2\rangle}{\langle|\boldsymbol{E}_{10}|^2\rangle}} \int_{V_c} \frac{|\boldsymbol{E}_{10}^*(\boldsymbol{r}) \cdot \boldsymbol{E}_a(\boldsymbol{r})|^2}{|\boldsymbol{E}_{10}|^2}\, dv \quad (41)$$

where we used (21a) to write the oscillating electric field of the ath mode as

$$\boldsymbol{E}_{\text{osc}}(\boldsymbol{r}) = -\frac{1}{\sqrt{\epsilon}}\, p_{a0}(\infty)\, \boldsymbol{E}_a(\boldsymbol{r})$$

and $\langle\ \rangle$ to denote spatial averaging over the crystal volume. We can now rewrite f as

$$f = \frac{f_0}{1 + \frac{\langle|\boldsymbol{E}_{\text{osc}}|^2\rangle}{\langle|\boldsymbol{E}_{10}|^2\rangle}} \quad (42)$$

where

$$f_0 = \int \frac{|\boldsymbol{E}_{10}^*(\boldsymbol{r}) \cdot \boldsymbol{E}_a(\boldsymbol{r})|^2}{|\boldsymbol{E}_{10}|^2}\, dv \quad (43)$$

and (37) becomes

$$\frac{1}{t_a} = \frac{2\epsilon_0 c\gamma_0 f_0}{\epsilon[1 + 4(\omega_1 - \omega_a)^2 t_a^2]} \left[\frac{1}{1 + \frac{\langle|\boldsymbol{E}_{\text{osc}}|^2\rangle}{\langle|\boldsymbol{E}_{10}|^2\rangle}}\right]. \quad (44)$$

The start oscillation condition is

$$\gamma_0 \geq \frac{n^2[1 + 4(\omega_1 - \omega_a)^2 t_a^2]}{2c\epsilon_0 f_0 t_a} \quad (45)$$

and does not depend on the pumping intensity $|\boldsymbol{E}_{i0}|^2$. This is a consequence of the index variation being driven by intensity moderation, not absolute intensity.

Equation (44) can be solved for the oscillating field intensity inside the resonator

$$\langle|\boldsymbol{E}_{\text{osc}}|^2\rangle = \langle|\boldsymbol{E}_{i0}|^2\rangle \left[\frac{2c\gamma_0 f_0 t_a n^{-2}}{1 + 4(\omega_1 - \omega_a)^2 t_a^2} - 1\right], \quad (46)$$

which is reminiscent of the expression for the power output of homogeneously broadened lasers [20].

We have neglected in our analysis the change in intensity of both the pump and resonator beams in the crystal due to the mutual power exchange. This neglect is well justified near threshold, and even a 20–30 percent power exchange per pass will not invalidate the basic conclusions of the above analysis. Another important issue is the relationship of distortion (or intentional spatial modulation) of the pumping beam $\boldsymbol{E}_{i0}$ on the oscillation. It follows from (43) that the main effect is to reduce the "projection" of $\boldsymbol{E}_{i0}$ on $\boldsymbol{E}_a$, leading to a smaller f_0 and thus, according to (45), to a higher threshold. The shape $\boldsymbol{E}_a(\boldsymbol{r})$ of the oscillating field is not affected.

This formalism can be generalized to include higher-

order modes of oscillation [21] and can be used to describe resonators with four-wave mixing gain (next section). In the latter case, the nonlinear polarization $\boldsymbol{P}_{\mathrm{NL}}$ must include all the grating terms involved in the interaction.

II. Four-Wave Mixing

The theory of four-wave mixing in photorefractive crystals has been developed recently [19]. The coupled wave equations describing the nonlinear system have been solved in the depleted pumps and single-grating approximations [22]–[24]. The theory was then used to describe novel self-pumped phase conjugate mirrors (PPCM's) [25]–[27]. In the following, we extend the theory to nondegenerate four-wave mixing, and we consider the PPCM's as photorefractively pumped oscillators: the phase conjugate pair of input/output beams pumps the oscillation between the crystal and some auxiliary mirrors (or the crystal itself). In particular, we shall discuss the oscillation conditions for the linear PPCM[28] and the cat-PPCM[27] in Section II-A, the semilinear PPCM [25] in Section II-B.

A. Linear Resonator

A linear resonator with photorefractive gain is shown in Fig. 6(a). A typical example of such an oscillator is the linear PPCM. The coupled wave equations describing photorefractive four-wave mixing in the slowly varying field approximation for the transmission grating without linear absorption are

$$\frac{dA_1}{ds} = -\gamma g A_4 \tag{47a}$$

$$\frac{dA_2^*}{ds} = -\gamma g A_3^* \tag{47b}$$

$$\frac{dA_3}{ds} = \gamma g A_2 \tag{47c}$$

$$\frac{dA_4^*}{ds} = \gamma g A_1^* \tag{47d}$$

where

$$g = (A_1 A_4^* + A_2^* A_3) \tag{48}$$

and A_j is the amplitude of beam j normalized by the square root of the conserved total average intensity $I_0 = I_1(s) + I_2(s) + I_3(s) + I_4(s)$.

Using the boundary conditions

$$I_1(0) = M_1 I_2(0) \tag{49}$$

and

$$I_2(l) = M_2 I_1(l) \tag{50}$$

we can obtain the intensity of oscillations, $I_1(0)$ and $I_2(l)$, and the phase conjugate reflectivity $R = I_3(0)/I_4(0)$ [7], [28],

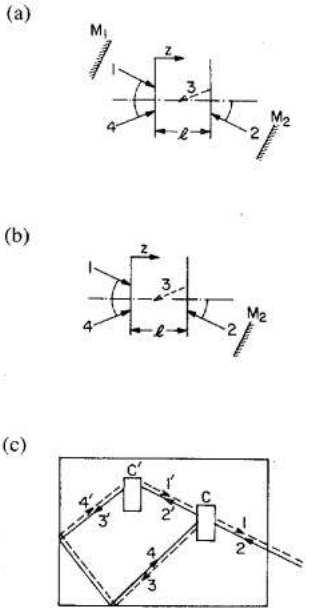

Fig. 6. Schematic diagrams. (a) Linear PPCM. (b) Semilinear PPCM. (c) cat-PPCM.

$$R = I_{34}(0) \tag{51}$$

$$I_2(l) = \frac{1 + \Delta}{2} \tag{52}$$

$$I_1(0) = \frac{I_{12}(0)}{2}\left[\frac{(1 + \Delta) - (1 - \Delta)\, I_{34}(0)}{1 - I_{12}(0)\, I_{34}(0)}\right] \tag{53}$$

where

$$I_{12}(s) \equiv \frac{I_1(s)}{I_2(s)} = \frac{1}{M_2}\left|\frac{T(s) + Q}{\Delta T(s) + Q + (1 + \Delta)\, T(s)/M_2}\right|^2 \tag{54}$$

$$I_{34}(s) \equiv \frac{I_3(s)}{I_4(s)} = \frac{(1 + \Delta)^2\, |T(s)|^2}{M_2\, |\Delta T(s) + Q|^2}$$

$$T(s) = \tanh\left(\frac{\gamma(l - s)}{2} Q\right)$$

$$Q = [\Delta^2 + (\Delta + 1)^2/M_2]^{1/2} \tag{57}$$

and the intensity flux $\Delta = I_2(l) - I_1(0) - I_4(0)$ is found from the solutions of the equation

$$M_1 M_2 = \left|\frac{T(0) + Q}{\Delta T(0) + Q + (1 + \Delta)\, T(0)/M_2}\right|^2 \tag{58}$$

where M_1 and M_2 are the intensity reflectivities of the cavity mirrors.

To examine the phases more effectively, we separate the amplitudes into magnitude and phase: $A_j = I_j^{1/2} \exp(i\psi_j)$. We write the roundtrip phase sum rule for the $M_1 - M_2$ cavity as

$$\varphi(l) - \varphi(0) + 2kL = 2\pi m \tag{59}$$

where m is an integer, L is the cavity length, and $\varphi(s) = \psi_1(s) - \psi_2(s)$. Since the observed frequency shift in pho-

torefractive processes is very small, we have neglected the frequency dependence of the wavenumber k.

To find the relationship between the detuning δ and cavity length L as given in (59), we rewrite (47a) and (47b) as

$$\frac{d \ln A_1}{ds} = -\gamma I_4(1 + \mathrm{f}) \tag{60a}$$

and

$$\frac{d \ln A_2^*}{ds} = -\gamma I_3(1 + 1/\mathrm{f}) \tag{60b}$$

where

$$\mathrm{f} = \frac{A_2^* A_3}{A_1 A_4^*}. \tag{61}$$

Taking the imaginary part of (60), we find

$$\frac{d\psi_1}{ds} = -\mathrm{Im}\,[\gamma I_4(1 + \mathrm{f})] \tag{62a}$$

and

$$\frac{d\psi_2}{ds} = \mathrm{Im}\,[\gamma I_3(1 + 1/\mathrm{f})] \tag{62b}$$

so that

$$\frac{d\varphi}{ds} = -\mathrm{Im}\,[\gamma I_4(1 + I_{34} + \mathrm{f} + I_{34}/\mathrm{f})] \tag{63}$$

where [28]

$$I_4(s) = \frac{1 - \Delta - I_{12}(s)(1 + \Delta)}{2(1 - I_{12}(s)\, I_{34}(s))} \tag{64}$$

and

$$\mathrm{f} = -\frac{(\Delta + 1)\, T(s)}{T(s) + Q}\left[1 + \frac{(\Delta + 1)\, T(s)}{M_2(\Delta T(s) + Q)}\right]. \tag{65}$$

The roundtrip phase condition (59) can be readily obtained by numerically integrating (63).

Note that if γ is real, then f is real, which implies [see (63)] that $d\varphi/ds = 0$. In this case, the phases of the oscillation beams are unaffected by the nonlinear interaction, and no compensation for cavity length detuning is possible.

Some typical plots of frequency shift δ and phase-conjugate reflectivity R versus cavity optical path length kL are given in Fig. 7. With $M_2 = 0.98$, we have shown what happens as M_1 is reduced towards zero, which is the case of the semilinear mirror. When M_1 is unity, then since the threshold coupling strength is very small, large amounts of detuning can be tolerated, and the phase conjugate reflectivity R even increases when the cavity length is slightly off resonance. However, only cavity detunings up to $\simeq 0.22\pi$ are possible. Since the quality factor of the oscillation cavity is quite high, the oscillation beams are significantly more intense than the signal beam, which is thus not very effective at transferring phase to the pumps. Therefore, not much cavity length detuning is allowed. As M_1 decreases, the oscillation beam becomes more dependent on continual replacement by the input beam. The phase of the oscillation beams depends more on the phase of the input beam and less on the phase of the oscillation beam returning to the crystal from M_1. Thus, a larger range of cavity length detunings is possible with smaller frequency detuning. Also, the oscillation condition begins to not allow the coupling constant to be complex. Eventually, when $M_1 = 0$, we reach the case of the semilinear PPCM, whose solution requires

$$T(0) + Q = 0,$$

which can only be satisfied if $T(0)$ is real, which implies γ is real, which in the absence of a uniform dc field E_0 implies $\delta = 0$ [see (5)]. M_1 is no longer present, and the roundtrip phase sum rule no longer needs to be satisfied.

The cat-PPCM may actually contain a linear PPCM [12]. A close-up picture of an operating cat-PPCM is shown in Fig. 8. Oscillation is observed between the lower left- and right-hand corners, connected by a total internal reflection at the upper surface. By applying black paint on the lower right-hand corner of the crystal the phase conjugate reflectivity is reduced by a factor of 100. This indicates that the oscillation between the lower left- and right-hand corners is effectively pumping the phase conjugate output. The origin of the cat-PPCM and its frequency detuning effect [29]–[31] are subjects of current investigation.

B. Phase Conjugate Resonators

A phase conjugate resonator (PCR) is an optical cavity bounded by a phase conjugate mirror (PCM) and an ordinary mirror. If the PCM exhibits sufficient gain to overcome the ordinary mirror and diffraction loss, an oscillating mode can be supported. The longitudinal and transverse modes of this device have been the subject of numerous theoretical and experimental investigations [32]–[37], and several important features, such as the existence of half-axial modes and the degeneracy of the transverse modes, distinguish the PCR from an ordinary resonator. Instabilities in the transverse mode of photorefractive PCR's have been observed, and the possibility that these instabilities represent chaos behavior is being currently investigated [14].

Here we analyze a semilinear PPCM as an example of a PCR with four-wave mixing gain. From Section II-A by putting the mirror $M_1 = 0$, we have already seen that there is no roundtrip phase requirement for such an oscillator.

From the theory of the transmission grating (58), the threshold may be obtained as

$$M_1 M_2 = \exp\,[(\gamma + \gamma^*) l]. \tag{66}$$

We see that no buildup of operation from zero oscillation strength is possible in the absence of mirror M_1 even when γl does have a real part. However, by providing a seed beam in the M_2 crystal cavity, such as feedback the fan-

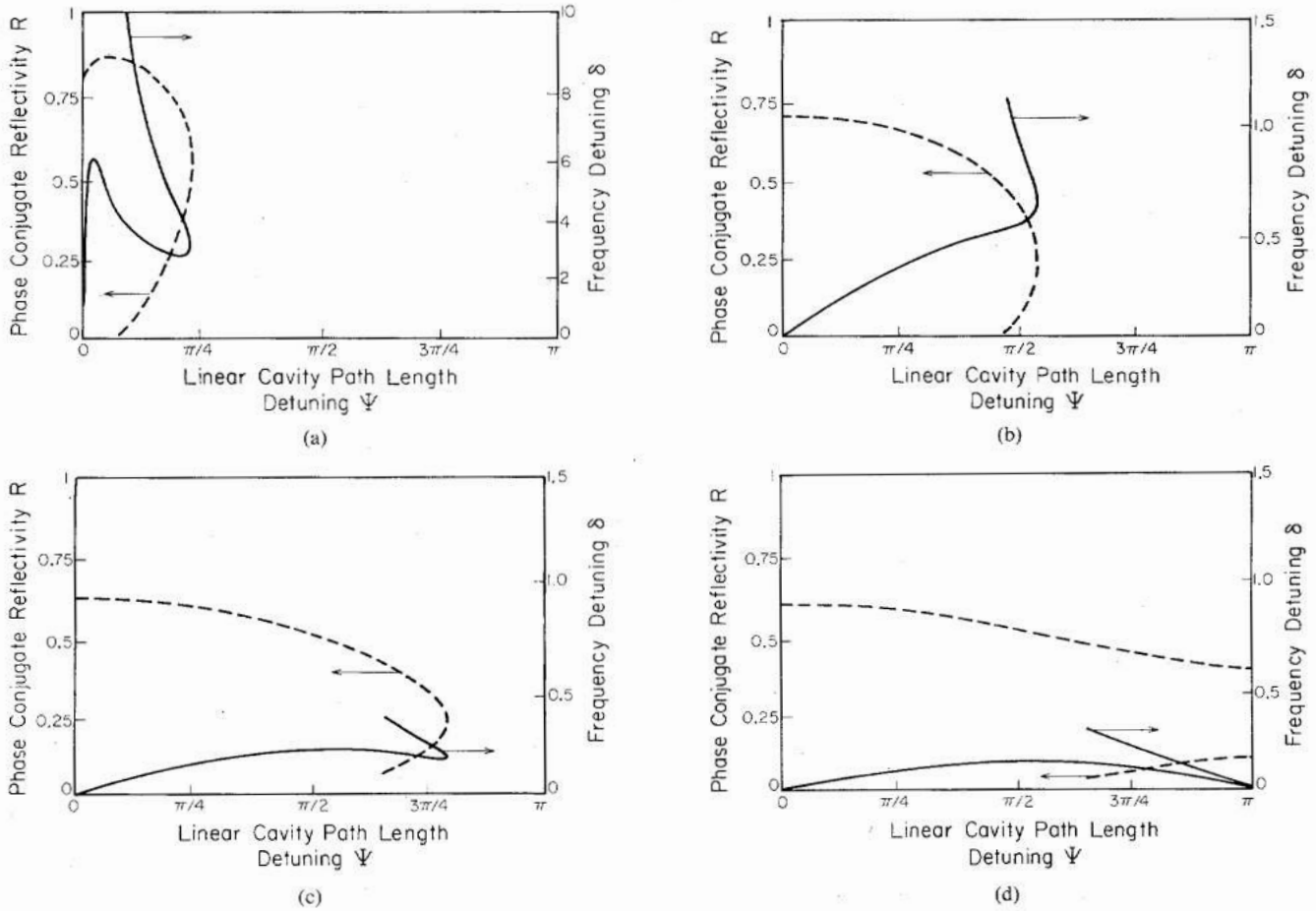

Fig. 7. Phase conjugate reflectivity R (dashes) and oscillation beam frequency detuning δ versus optical path length kL modulo 2π in empty oscillation cavity. Only the path length range 0 to π is shown: the results show natural symmetry about the origin. In each case, the undetuned coupling constant $(\gamma l)_o = -3$ and $M_2 = 0.98$. The detuning δ is normalized by the constant quantity $I_4(0)/(I_o\tau)$. M_1 varies as follows. (a) 1.00. (b) 0.125. (c) 0.025. (d) 0.01. Note the change of scale in δ for (b), (c), and (d).

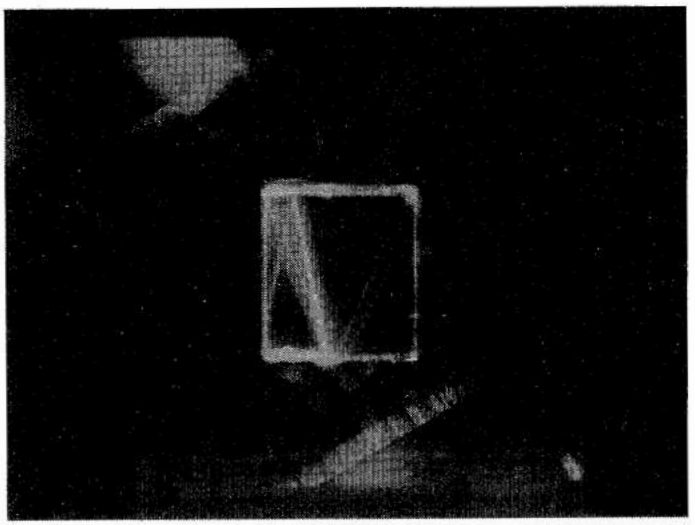

Fig. 8. Picture of an operating cat-PPCM.

ning by a curved mirror, it is possible to build up oscillation in the absence of mirror M_1.

With $M_1 = 0$, (58) implies that

$$\tanh\left[-\frac{\gamma l}{2}\left[\Delta^2 + (\Delta + 1)^2/M_2\right]^{1/2}\right] = \left[\Delta^2 + (\Delta + 1)^2/M_2\right]^{1/2}, \tag{67}$$

so that Δ may found from the solution of the quadratic equation

$$\Delta^2 + \frac{(\Delta + 1)^2}{M_2} = a^2 \tag{68}$$

where a is simply related to the coupling constant γl by

$$\tanh\left[-\frac{\gamma l}{2}a\right] = a. \tag{69}$$

The oscillation intensity is

$$I_2(l) = \frac{(1 + \Delta)}{2}. \tag{70}$$

The phase conjugate reflectivity can be written, using (55), in closed form as

$$R = \left[\frac{M_2^{1/2} \pm [a^2(1 + M_2) - 1]^{1/2}}{M_2 + 2 \mp M_2^{1/2}[a^2(1 + M_2) - 1]^{1/2}}\right]^2, \quad (71)$$

so that the device is at threshold with reflectivity $R = R_t$,

$$R_t = \frac{M_2}{(M_2 + 2)^2}, \quad (72)$$

when a^2 equals a_t^2,

$$a_t^2 = \frac{1}{(1 + M_2)}. \quad (73)$$

In terms of γ this threshold is given by

$$(\gamma l)_t = (1 + M_2)^{1/2} \ln\left[\frac{(1 + M_2)^{1/2} - 1}{(1 + M_2)^{1/2} + 1}\right]. \quad (74)$$

It is possible to show that of the two possible values of the above threshold reflectivity (71) only the one associated with the upper sign is stable.

C. Double Phase Conjugate Resonator

A double phase conjugate resonator [24], [38], and [39] exhibits additional complexity as the nonlinear media as well as the intensities and phases of the pumping beams may be different in each PCM. This leads to fundamental differences between the single and double phase conjugate resonators. In the following paragraphs we present experimental and theoretical results concerning the nondegenerate oscillation, which we have observed to be strongly dependent on the phases of the pumping beams.

Consider the propagation of a probe beam traveling between two PCM's pumped at different frequencies. Suppose we pump the first PCM (PCM_1) at frequency ω_1 and the second PCM (PCM_2) at ω_2. Without loss of generality we assume the probe to be traveling initially towards PCM_2 and to have frequency ω. Using the frequency-flipping character of PCM's ($\omega_{pump} + \delta \rightarrow \omega_{pump} - \delta$) we find that after one roundtrip, the probe frequency has become $\omega + 2(\omega_1 - \omega_2)$. After sufficient roundtrips, the frequency of the probe would walk off the gain spectrum of both PCM's. In practice, this means that oscillation between two PCM's is not possible unless the mirrors are pumped by lasers whose frequency spectra overlap appreciably. If at least one of the PCM's is self-pumped [39], this condition will be satisfied automatically.

With this in mind, we analyze oscillation between a pair of PCM's pumped at the same frequency ω. Allowing for possible nondegenerate oscillation we write the frequency of the field propagating from PCM_1 to PCM_2 as $\omega - \delta$, with $\omega + \delta$ being the frequency of the field traveling in the opposite direction. The net accumulated roundtrip phase change is $\phi_2(-\delta) - \phi_1(\delta) + 2\delta L/c$ where $\phi_i(\delta)$ is the phase change upon reflection from PCM_i and L is the cavity length. A self-consistent oscillation must satisfy

$$\phi_2(-\delta) - \phi_1(\delta) + 2\delta L/c = 2m\pi \quad (75)$$

where m is an integer.

Each of the phase shifts ϕ_i is due to two separate physical effects. The first is a dependence on the combined phases of the pumping beams. The amplitudes of the three input beams are essentially multiplied to give the amplitude of the phase conjugate reflection: hence, the pump phases ψ_1 and ψ_2 are added to the reflected wave. The second effect involves the internal physics of the crystal. When the probe beam frequency is offset from that of the pump beams, the refractive index grating responsible for beam coupling moves in space in synchronism with the light interference pattern. The finite response time of the medium implies a phase lag Θ between the interference pattern and the index grating [40]–[42].

In the undepleted pumps approximation, the phase shift ϕ_i at mirror i is

$$\phi_i(\delta) = \psi_{1i} + \psi_{2i} + \Theta_i(\delta). \quad (76)$$

As an example, Θ for a photorefractive phase conjugate mirror is given by [19]

$$\Theta = \text{Im} \ln \frac{\sinh\left(\frac{\gamma l}{2}\right)}{\cosh\left(\frac{\gamma l}{2} + \frac{\ln r}{2}\right)} \quad (77)$$

where r is the ratio of the intensities of the two pumping beams.

To see the underlying physics of the device more clearly, we assume that both PCM's are the same except for the phases of the pumping beams, so that $\Theta_1 = \Theta_2 = \Theta$. Since in the photorefractive case Θ is an odd function of δ, (75) can be rewritten as

$$-\Psi - 2\Theta(\delta) + 2\delta L/c = 2\pi m \quad (78)$$

where $\Psi = \psi_{11} + \psi_{21} - \psi_{12} - \psi_{22}$. We see that, except for the special case $\Psi = 0$, δ must be nonzero. It also follows from (78) that the δ is periodic in Ψ and L.

In our experiment, the response time of the photorefractive medium was much greater than the cavity roundtrip time, so that the term $2\delta L/c$ in (78) is negligible. Fig. 9 shows the theoretically predicted frequency offset δ and the associated phase conjugate reflectivity as a function of Ψ with $\gamma_0 l = -3$. We note that, while it is the oscillation intensity and not the undepleted phase conjugate reflectivity that is measured in the experiment, these two quantities should be at least qualitatively similar.

Fig. 10 is a schematic of our experimental arrangement. The output of an argon ion laser running in single longitudinal mode at 514.5 nm was divided at beamsplitter BS into two beams of equal intensity which pumped two crystals of $BaTiO_3$ as PCM's. The second set of two pumping beams, one for each PCM, was provided by retroreflecting mirrors M_1 and M_2. Mirror M_1 was on a piezomount so that the combined pumping beam phase Ψ could be controlled by its position. The crystal orientations were chosen so that the reflectivity of each PCM to a beam arriving from the other was greater than unity. Oscillation beams built up in the double phase conjugate

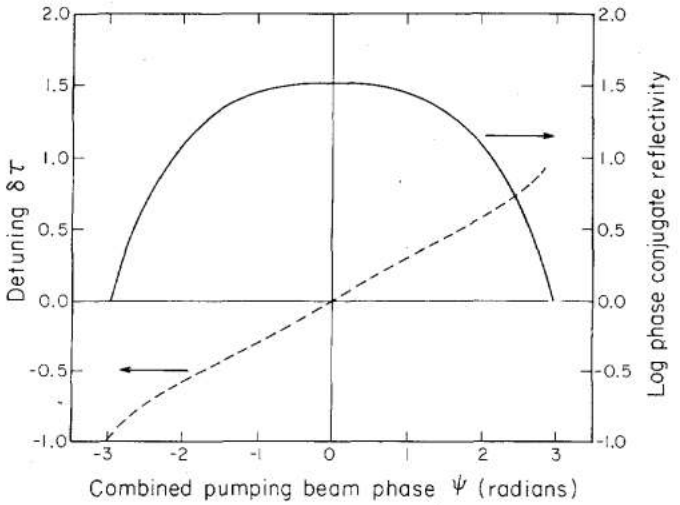

Fig. 9. Theoretical plot of frequency detuning in double-conjugate conjugate resonator and associated reflectivity of the phase conjugate mirrors of which it is composed. The coupling constant $\gamma_o l$ for each mirror equals 3. The undepleted pumps approximation is used.

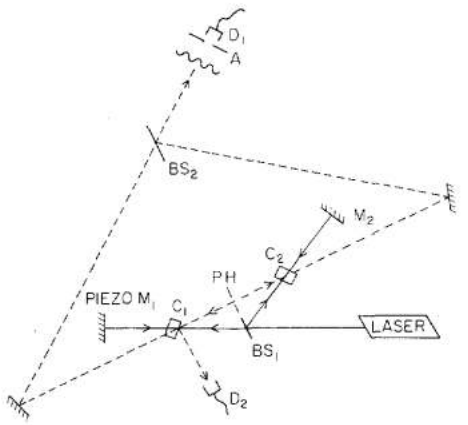

Fig. 10. The experimental arrangement used to demonstrate oscillation detuning in the double phase conjugate resonator. An argon ion laser was used at 514.5 nm in single longitudinal and TEM_{00} modes. The power output was 100 mW. Using a Cartesian coordinate system with the abscissa coincident with the beam leaving, the laser locations of the elements in centimeters were: beam splitter BS_1 (0, 0), $BaTiO_3$ crystal C_1 of PCM_1 (−8.9, 0), $BaTiO_3$ crystal C_2 of PCM_2 (8.9, 7.6), piezomirror M_1 (−19, 0), mirror M_2 (17.8, 15.3). The c-axis of C_1 pointed in the direction of the vector (0.95, −0.30), the c-axis of C_2 in the direction (0.91, −0.42). The c-axis is defined here as pointing towards the surface which had been connected to the negative electrode at poling. A 100 μm pinhole PH was inserted in the resonator to stabilize the oscillation. Detector D_1 was placed behind aperture A at the output of the interferometer to measure the detuning. Detector D_2 monitored the oscillation intensity using a Fresnel reflection from the surface of crystal C_1.

resonator, and the parts of these beams transmitted through the crystals, were made to interfere with each other. Detector D_1 was used to measure the fringe speed from which the detuning δ was inferred. Detector D_2 gave the oscillation intensity. A 100 μm pinhole was used to stabilize oscillation in the resonator [14]. The frequency detuning and oscillation intensity showed periodicity in Ψ with period 2π (or equivalently in L with period $\lambda/2$). Fig. 11 shows one period of detuning δ and the oscillation intensity as a function of the combined pumping phase Ψ. We have also performed experiments in which we beat

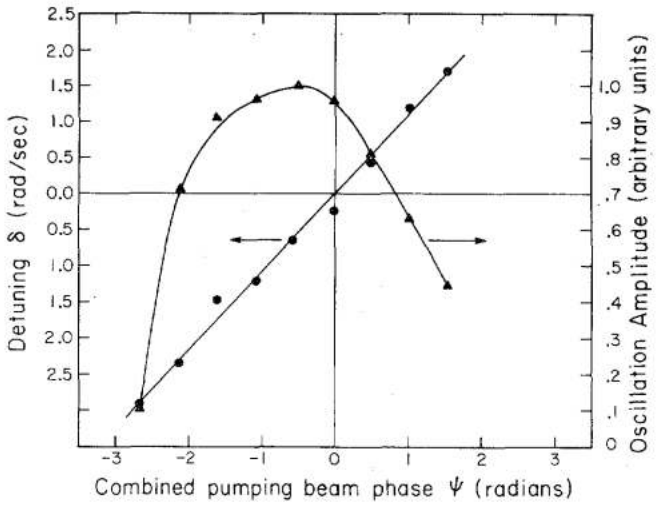

Fig. 11. The experimental results showing the detuning and oscillation intensity as a function of the combined pumping beam phase derived from the position of piezomirror M_1.

the oscillation beams directly against light at the pump frequency ω_{pump} split directly off the laser output. The detunings were equal and opposite in sign, consistent with the theory.

III. Applications

In this section, we discuss two applications of the resonators with photorefractive gain: a) optical-path-length-to-frequency conversion interferometer and b) one-way real-time wavefront converters. Other applications, such as distortion correction in laser cavities [43], laser gyroscopes [15], [44], bistability [45], [46], associative memories [47]–[49], and self-scanning of a CW dye laser [29], [30], [50], have been reported separately.

A. Optical-Path-Length-to-Frequency Conversion Interferometers

In traditional interferometry, changes in optical path length cause changes in fringe position at the output of an interferometer. This change in fringe position is inferred by intensity-measuring detectors. The precision of these devices might thus be limited by the precision with which intensity measurements can be made.

Frequency can often be measured with much higher precision than intensity. Therefore, an interferometer whose output can be measured by a frequency counter will benefit from this improved precision. Many types of photorefractive oscillator, including the ring resonator, the double phase conjugate resonator, and the linear PPCM, can be used in this manner [5].

B. One-Way Real-Time Wavefront Converters

Many laser systems give rise to highly distorted laser beams. The distortion is due mostly to optical "imperfections" and aberrations in the laser resonator (including those of the pumped gain medium) or in transmission through a distorting medium. The question arises as to the

possibility of beam "cleanup," i.e., of improving the spatial properties of the beam, in real time.

A number of schemes were described recently in which stimulated Raman scattering (SRS) was used to amplify a "clean" Stokes seed beam by a highly distorted pump beam [51]. The basic physical idea is that power can be transferred continuously from the distorted pump beam to the Stokes beam without transferring the phase, i.e., distortion of the former. The distortion phase increment is transferred instead to the locally excited molecular vibration.

The mathematical nature of the Raman (or Brillouin) nonlinearity is similar to that of the photorefractive effect. In each of these, the presence of two beams

$$\boldsymbol{E}_1(\boldsymbol{r}, t) = \tfrac{1}{2}\boldsymbol{E}_{10}(\boldsymbol{r})\, e^{i(\omega_1 t - \boldsymbol{k}_1 \cdot \boldsymbol{r})} + c.c. \tag{79a}$$

and

$$\boldsymbol{E}_2(\boldsymbol{r}, t) = \tfrac{1}{2}\boldsymbol{E}_{20}(\boldsymbol{r})\, e^{i(\omega_2 t - \boldsymbol{k}_2 \cdot \boldsymbol{r})} + c.c. \tag{79b}$$

gives rise to a nonlinear polarization (31)

$$P_{\mathrm{NL}}(\boldsymbol{r}, t) = \frac{i\gamma'(\boldsymbol{E}_{10}^{*} \cdot \boldsymbol{E}_{20})\boldsymbol{E}_{10}}{1 + i[(\omega_1 - \omega_2) - \omega']\tau}\, e^{i(\omega_2 t - \boldsymbol{k}_2 \cdot \boldsymbol{r})} + c.c. \tag{80}$$

where ω' is some characteristic frequency of the medium, τ is a damping time, and γ' represents the strength of the coupling between $\boldsymbol{E}_{10}$ and $\boldsymbol{E}_{20}$, which is related to the physical mechanism of the nonlinear interaction and where for the sake of simplicity we adopted scalar notation. The imaginary part of P_{NL}, in quadrature with $\boldsymbol{E}_{20}$, gives rise to an amplification of $\boldsymbol{E}_{20}$ (the Stokes beam) by $\boldsymbol{E}_{10}$. This polarization then radiates, thus causing transfer of power from ω_1 to ω_2.

This formal similarity between SRS and photorefractive two-beam coupling suggests that one can achieve beam cleanup using photorefractive nonlinear optical techniques. An advantage of using a photorefractive medium is that it can be operated at low power, milliwatts, while SRS requires high beam power to reach the threshold.

In our experiment the cleaned up beam does not result from injecting and amplifying a seed input, but is self-generated by a mode of an optical resonator which is pumped by the distorted beam. The experimental setup is similar to that in Fig. 12. The distorted pump beam $\boldsymbol{E}_{10}$ is incident on a poled $BaTiO_3$ crystal placed inside a ring oscillator. The photorefractive two-beam coupling described in Section I provides gain, which enables a mode $\boldsymbol{E}_{20}$ of the ring resonator to oscillate. The spatial characteristics of the mode $\boldsymbol{E}_{20}$ are determined by the resonator, and ideally not the pump beam, thus leading to beam cleanup.

A fundamental figure of merit for the wavefront converter is the ratio G of the photometric brightness (W/m^2-Sr) of the output beam to that of the input. This ratio is

$$G = \left(\frac{P_o}{P_i}\right)\left(\frac{\theta_i}{\theta_o}\right)^2\left(\frac{A_i}{A_o}\right) \tag{81}$$

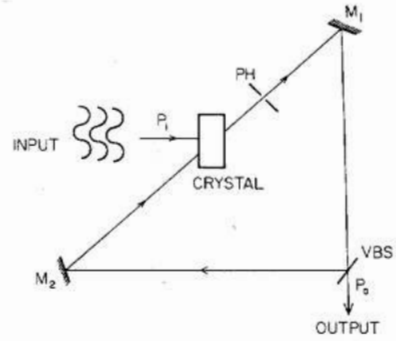

Fig. 12. Schematic diagram of a wavefront converter.

where θ_o and θ_i refer to the beam spreading angle at the output and input, respectively, and $A_{o,i}$ and $P_{o,i}$ are the respective beam diameters and powers. We note that in passive optical systems, $G < 1$.

In the experiment, a TEM_{00} mode argon laser beam (514.5 nm, 50 mW, beam diameter 1.5 mm, and beam divergence 0.5 mrad) passed through a distorting medium[1] which caused the beam divergence to increase to about 50 mrad. A ring resonator ($L = 40$ cm) was placed about 5 cm behind the distortion medium. The ring resonator consists of two 99 percent reflecting mirrors, a variable beam splitter (VBS) serving as the output coupler, and a poled $BaTiO_3$ crystal. By introducing an intracavity aperture with a diameter <0.4 mm, the high-order modes of the ring resonator were suppressed and oscillation in a steady TEM_{00}-like mode resulted. Several types of distorting media (both thin and thick) have been used.

The very considerable improvement in the spatial characteristics of the mode is evident in a comparison between Fig. 13(g) and (h). The output (oscillating beam) beam has beam waist and divergence equal to 0.4 mm and 1.15 mrad, respectively. The maximum power conversion efficiency $\eta = P_o/P_i$ measured was 15 percent, which corresponds to a wavefront conversion figure of merit $G = 4000$. This is to be compared to the results using spatial filtering techniques, which yield $\eta < 0.1$ percent and $G < 1$.

The power conversion efficiency η of the wavefront converter can be calculated from a recent theory for photorefractively pumped oscillators [4], [11]. Such a theory leads to a result[2]

$$\eta = \frac{(1 - R)}{R}\,\frac{1 - \exp\left(-2\gamma_0 l f_0 \dfrac{\gamma_o L f_o}{1 + 4(\omega_2 - \omega_1)^2 t_a^2}\right)}{1 - Re^{-\alpha l}} \tag{82}$$

where ω_1 and ω_2, we recall, are the frequencies of the pump and the oscillation beam, respectively, t_a is the photon lifetime of the passive ring resonator, and f_0 is the overlap integral given by (43). We note that the effect of

[1]The distortion media used in these experiments were prepared by etching pieces of glass (1 mm thickness) in 48 percent HF acid for 1 min.

[2]Equation (82) reduces to (46) in the undepleted pump approximation and reduces to (11) in plane wave approximation.

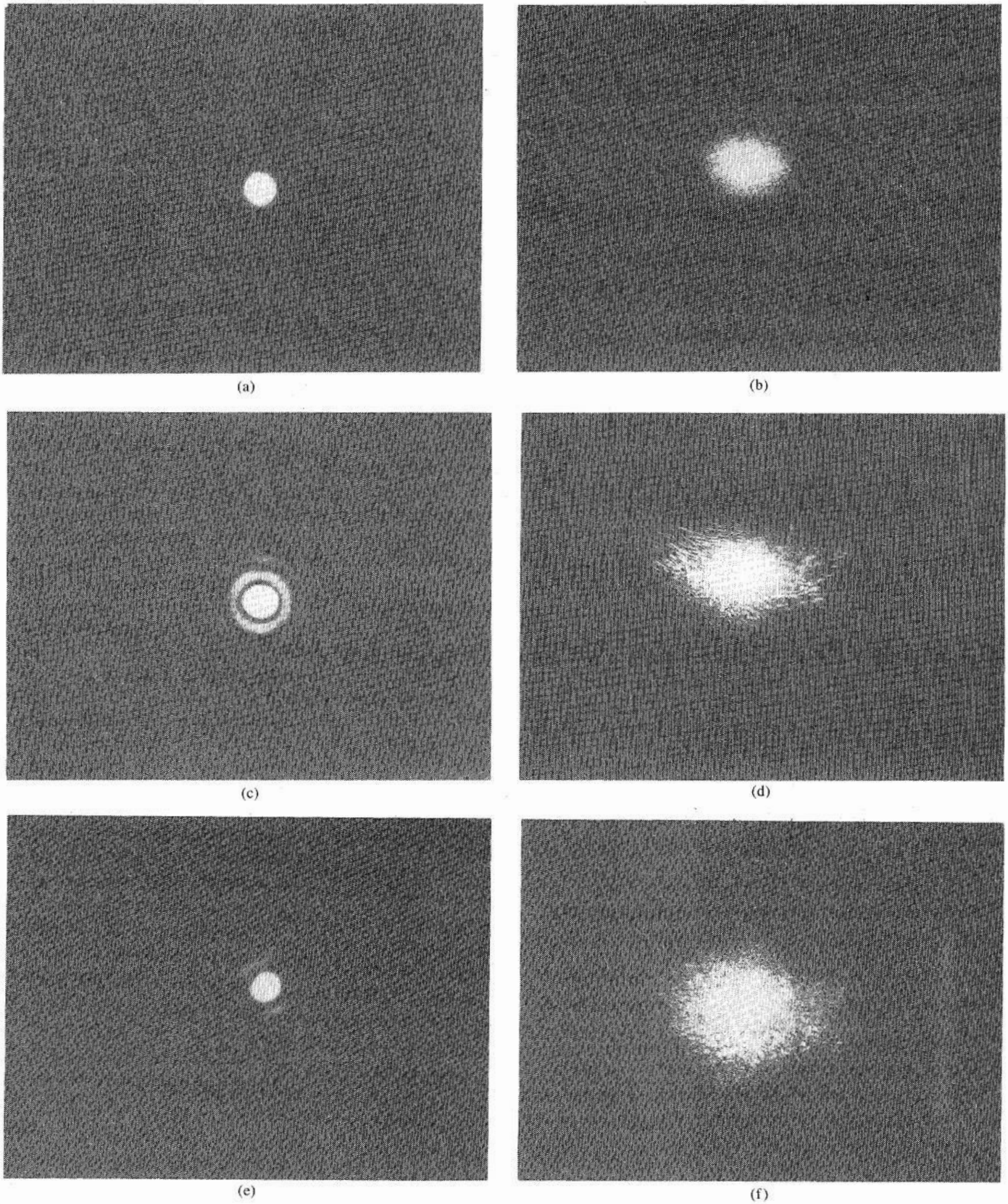

Fig. 13. (a) Undistorted laser beam. (b) Laser beam after passing through a distortion medium without correction. (c) The corresponding corrected output beam. (d) Laser beam after passing through a distortion medium formed by two pieces of etched glass stacked together. (e) The corresponding corrected output beam. (f) Laser beam after passing through a thick distortion formed by three pairs of etched glass, each of them separated by 1 in. (g) The corresponding corrected output beam.

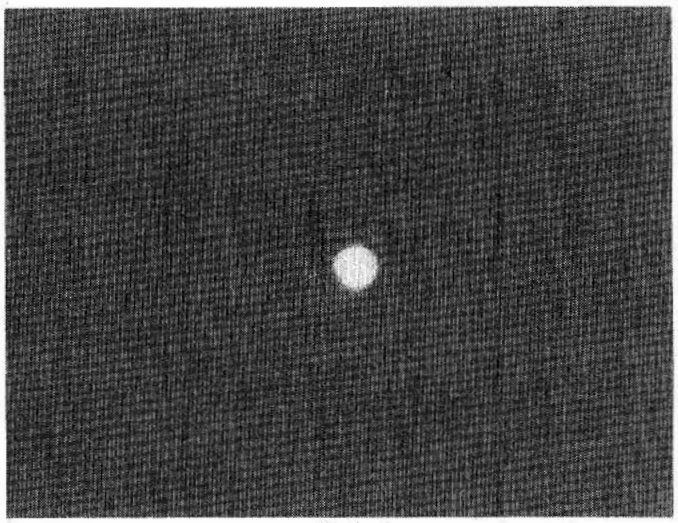

(g)

Fig. 13. (*Continued.*)

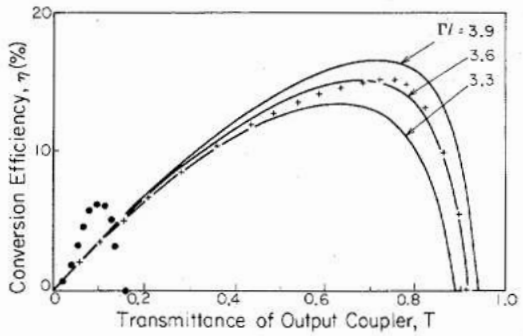

Fig. 14. Conversion efficiency η versus transmittance $T = 1 - R$ of the output coupler (VBS). (+) and (•) are experimental points using ring oscillator (Fig. 12) and ring PPCM [Fig. 17(d)]. The continuous lines are theoretical plots based on (82) for $\alpha l = 1.11$, and $\Gamma l = 3.3$, 3.6, and 3.9

distortion of the pump beam $\boldsymbol{E}_{10}$ is to reduce the "projection" of $\boldsymbol{E}_{10}$ on $\boldsymbol{E}_{20}$, leading to a smaller f_0 and thus to a smaller conversion efficiency.

Fig. 14 shows a plot of the measured power conversion efficiency of our device as well as the theoretical values from (82). We defined the modified coupling constant Γl as

$$\Gamma l = \frac{2\gamma_0 l f_0}{[1 + 4(\omega_2 - \omega_1)t_2^2]^2}. \tag{83}$$

The theoretical curves agree quite well with experimental data when $\alpha l = 1.11$ and $\Gamma l = 3.6$. From independent experiments, we also measured $\alpha l = 1.11$ and $\Gamma l = 3.4$.

From (82), the maximum conversion efficiency $\eta_{\max}$ is derived for given αl and Γl

$$\eta_{\max} = \frac{(e^{-\alpha l} + e^{-\Gamma l})\,[1 + \sqrt{1 - e^{\alpha l} - e^{\Gamma l} + e^{(\alpha l + \Gamma l)}}] - 2}{\sqrt{1 - e^{\alpha l} - e^{\kappa'} + e^{(\alpha l + \Gamma l)}} - 1} \tag{84}$$

at the transmittivity of the output coupler, $R_{\max}$,

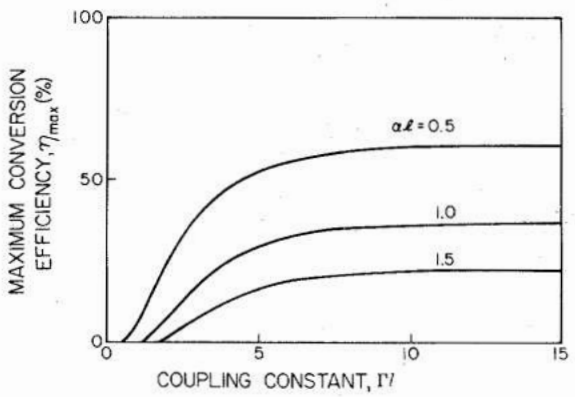

Fig. 15. Maximum conversion efficiency $\eta_{\max}$ versus modified coupling constant Γl with $\alpha l = 0.5$, 1.0, 1.5.

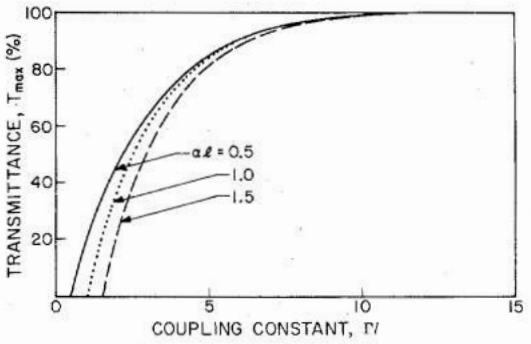

Fig. 16. Transmittivity of output coupler at maximum conversion efficiency $T_{\max}$ versus coupling constant Γl.

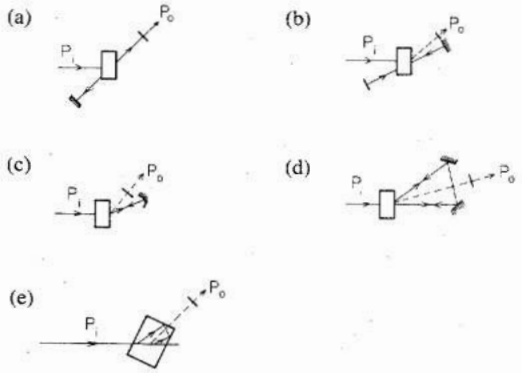

Fig. 17. Wavefront converters using other oscillation configurations. (a) Linear PPCM with output taken from the self-induced pumping beam. (b) Linear PPCM with a self-induced oscillation. (c) Semilinear PPCM with a self-induced oscillation. (d) Ring PPCM with a self-induced oscillation. (e) Two-interaction-region PPCM with a self-induced oscillation.

$$T_{\max} = 1 - \frac{e^{-\kappa'}[1 - \sqrt{1 - e^{\alpha l} - e^{\kappa'} + e^{(\alpha l + \kappa')}}]}{e^{-\alpha l} + e^{-\kappa'} - 1}. \tag{85}$$

Theoretical plots of $\eta_{\max}$ and $T_{\max}$ as a function of Γl for various αl are shown in Figs. 15 and 16, respectively. We note that $\eta_{\max}$ is saturated for given αl. On the other hand, however, the αl should not be too small because it is required for the photorefractive effect.

We have also employed other resonator configurations instead of a ring oscillator (Fig. 17). These included the

linear, the semilinear, the ring cavity, and the two-interaction-region self-pumped phase conjugate mirrors. They all led to impressive spatial mode cleanup, but with smaller power conversion ($\simeq 6$ percent). This may be due to the fact that in these cases a good deal of power is phase conjugated back to the pump. One advantage of the devices in Fig. 15(c) and (d) is that they can be pumped with light sources of short coherent length or even with mode-locked laser light [53]. This is because of the semilinear and the ring PPCM used in dynamic transmission holograms, which are insensitive to vibration.

The small frequency shift (Section I) between the pump and the oscillating beam which exists in these oscillators (a few hertz) is probably of little consequence in most practical situations, but should be noted.

Conclusion

In summary, we have used two different points of view to develop theoretical models of oscillators with photorefractive gain. The first is a plane-wave analysis which retains the nonlinearities in the coupled wave equations governing transfer of power from pump to oscillation beams. The second is a general laser treatment which linearizes the equations but retains the effects of transverse variation in the amplitudes of the pump and the oscillation modes. This yields threshold conditions based on the amount of spatial overlap between these beams. Both theories describe the frequency detuning effects which have been the subject of much current research in photorefractive devices. We have applied these theories to several photorefractive oscillators: the unidirectional ring resonator, the linear passive phase conjugate mirror, a phase conjugate resonator, and a double phase conjugate resonator. Finally, an understanding of these processes has led to several applications, two of which we have described here: an optical-path-length-to-frequency converting interferometer and one-way real-time wavefront converters.

Acknowledgment

The authors would like to acknowledge helpful discussions with J. O. White. This work was supported by the U.S. Air Force Office of Scientific Research and the U.S. Army Research Office, Durham, North Carolina.

References

[1] N. V. Kukhtarev, V. B. Markov, S. G. Odulov, M. S. Soskin, and V. L. Vinetskii, "Holographic storage in electrooptic crystals. I. Steady state," *Ferroelect.*, vol. 22, pp. 949–960, 1979.

[2] J. Feinberg, D. Heiman, A. R. Tanguay, Jr., and R. W. Hellwarth, "Photorefractive effects and light induced charge migration in barium titanate," *J. Appl. Phys.*, vol. 51, pp. 1297–1305, 1980.

[3] N. V. Kukhtarev, V. B. Markov, S. G. Odulov, M. S. Soskin, and V. L. Vinetskii, "Holographic storage in electrooptic crystals. II. Beam coupling—Light amplification," *Ferroelect.*, vol. 22, pp. 961–964, 1979.

[4] V. L. Vinetskii, N. V. Kukhtarev, S. G. Odulov, and M. S. Soskin, "Dynamic self-diffraction of coherent light beams," *Sov. Phys. Usp.*, vol. 22, p. 742–756, 1979.

[5] S. K. Kwong, A. Yariv, M. Cronin-Golomb, and I. Ury, "Optical path length to frequency converting interferometer using photorefractive oscillation," *Appl. Phys. Lett.*, vol. 47, pp. 460–462, 1985.

[6] P. Yeh, "Theory of unidirectional photorefractive ring oscillation," *J. Opt. Soc. Amer. B*, vol. 2, 1924–1928, 1985.

[7] D. W. Vahey, "A nonlinear coupled-wave theory of holographic storage in ferroelectric materials," *J. Appl. Phys.*, vol. 46, pp. 3510–3515, 1975.

[8] M. Cronin-Golomb, "Large nonlinearities in four-wave mixing in photorefractive crystals and applications in passive optical phase conjugation," Ph.D. dissertation, California Institute of Technology, Pasadena, CA, 1983, unpublished.

[9] J. P. Huignard and A. Marrackchi, "Coherent signal beam amplification in two-wave mixing experiments with photorefractive $Bi_{12}SiO_{20}$ crystals," *Opt. Commun.*, vol. 38, pp. 249–254, 1981.

[10] J. O. White, M. Cronin-Golomb, B. Fischer, and A. Yariv, "Coherent oscillation by self-induced gratings in the photorefractive crystal $BaTiO_3$," *Appl. Phys. Lett.*, pp. 450–452, 1982.

[11] A. Yariv and S. K. Kwong, "Theory of laser oscillation in resonators with photorefractive gain," *Opt. Lett.*, vol. 10, pp. 454–456, 1985.

[12] M. Ewbank and P. Yeh, "Frequency shift and cavity length in photorefractive resonators," *Opt. Lett.*, vol. 10, pp. 496–498, 1985.

[13] H. Rajbenbach and J. P. Huignard, "Self-induced coherent oscillations with photorefractive $Bi_{12}SiO_{20}$ amplifier," *Opt. Lett.*, vol. 10, pp. 137–139, 1985.

[14] G. C. Valley and G. J. Dunning, "Observation of chaos in a phase-conjugate resonator," *Opt. Lett.*, vol. 9, pp. 513–515, 1984.

[15] P. Yeh, "Photorefractive coupling in ring resonators," *Appl. Opt.*, vol. 23, pp. 2974–2978, 1984.

[16] W. E. Lamb, Jr., "Theory of an optical maser," *Phys. Rev.*, vol. *134*, no. (6A), pp. A1429–A1439, 1964.

[17] A. Yariv, *Quantum Electronics*, 2nd ed. New York: Wiley, 1975.

[18] J. C. Slater, *Microwave Electronics*. Princeton, NJ: Van Nostrand, 1950.

[19] B. Fischer, M. Cronin-Golomb, J. O. White, and A. Yariv, "Amplified reflection transmission, and self-oscillation in real-time holography," *Opt. Lett.*, vol. 6, pp. 519–521, 1981.

[20] A. Yariv, *Optical Electronics*, 3rd ed. New York: Holt, Rinehart and Winston, 1985, p. 159, eq. (6.4-13).

[21] D. Z. Anderson and R. Saxena, in *Tech. Dig., Opt. Soc. Amer. 1985 Annu. Meet.*, 1985.

[22] M. Cronin-Golomb, J. O. White, B. Fischer, and A. Yariv, "Exact solution of a nonlinear model of four-wave mixing and phase conjugation," *Opt. Lett.*, vol. 7, pp. 313–315, 1982.

[23] M. Cronin-Golomb, B. Fischer, J. O. White, and A. Yariv, "Theory and applications of four-wave mixing in photorefractive media," *IEEE J. Quantum Electron.*, vol. QE-20, pp. 12–30, 1984.

[24] S. K. Kwong, M. Cronin-Golomb, B. Fischer, and A. Yariv, "The phase of phase conjugation and its effect in the double phase conjugate resonator," *J. Opt. Soc. Amer. A*, vol. 3, pp. 157–160, 1986.

[25] M. Cronin-Golomb, B. Fischer, J. O. White, and A. Yariv, "Passive (self-pumped) phase conjugate mirror: Theoretical and experimental investigations, *Appl. Phys. Lett.*, vol. 41, pp. 689–691, 1982.

[26] M. Cronin-Golomb, B. Fischer, J. O. White, and A. Yariv, "Passive phase conjugate mirror based on self-induced oscillation in an optical ring cavity," *Appl. Phys. Lett.*, vol. 42, pp. 919–921, 1983.

[27] J. Feinberg, "Self-pumped, continuous-wave phase conjugator using internal reflection," *Opt. Lett.*, vol. 7, pp. 486–488, 1982; K. MacDonald and J. Feinberg, "Theory of a self-pumped phase conjugator with two coupled interaction regions," *J. Opt. Soc. Amer.*, vol. 73, pp. 548–553, 1983.

[28] M. Cronin-Golomb and A. Yariv, "Plane wave theory of nondegenerate oscillation in the linear photorefractive passive phase conjugate mirror," *Opt. Lett.*, to be published.

[29] W. B. Whitten and J. M. Ramsey, "Self-scanning of a dye laser due to feedback from a $BaTiO_3$ phase-conjugate reflector," *Opt. Lett.*, vol. 9, pp. 44–46, 1984.

[30] J. Feinberg and G. D. Bacher, "Self-scanning of a continuous-wave dye laser having a phase-conjugating resonator cavity," *Opt. Lett.*, vol. 9, pp. 420–422, 1984.

[31] P. Gunter, E. Voit, and M. Z. Zha, "Self-pulsation and optical chaos in self-pumped photorefractive $BaTiO_3$," *Opt. Commun.*, vol. 55, pp. 210–214, 1985.

[32] J. AuYeung, D. Fekete, D. M. Pepper, and A. Yariv, "A theoretical and experimental investigation of the modes of optical resonators with phase-conjugate mirrors," *IEEE J. Quantum Electron.*, vol. QE-15, pp. 1180–1188, 1979.

[33] I. M. Bel'dyugin and E. M. Zemskov, "Properties of resonators with wavefront-reversing mirrors," *Sov. J. Quantum Electron.*, vol. 9, pp. 1198–1199, 1979.

[34] J. F. Lam and W. P. Brown, "Optical resonators with phase-conjugate mirrors," *Opt. Lett.*, vol. 5, pp. 61–63, 1980.
[35] P. A. Belanger, A. Hardy, and A. E. Siegman, "Resonant modes of optical cavities with phase conjugate mirrors: High-order modes," *Appl. Opt.*, vol. 19, pp. 479–480, 1980.
[36] P. A. Belanger, A. Hardy, and A. E. Siegman, "Resonant modes of optical cavities with phase-conjugate mirrors," *Appl. Opt.*, vol. 19, pp. 602–609, 1980.
[37] M. G. Reznikov and A. I. Khizhnyak, "Properties of a resonator with a wavefront-reversing mirror," *Sov. J. Quantum Electron.*, vol. 10, pp. 633–634, 1979.
[38] M. Cronin-Golomb, B. Fischer, S. K. Kwong, J. O. White, and A. Yariv, "Nondegenerate optical oscillation in a resonator formed by two phase-conjugate mirrors," *Opt. Lett.*, vol. 10, pp. 353–355, 1985.
[39] M. D. Ewbank, P. Yeh, M. Khoshnevisan and J. Feinberg, "Time reversal by an interferometer with coupled phase-conjugate reflectors," *Opt. Lett.*, vol. 10, pp. 282–284, 1985.
[40] S. I. Stepanov, V. V. Kulikov, and M. P. Petrov, "'Running' holograms in photorefractive $Bi_{12}SiO_{20}$ crystals," *Opt. Commun.*, vol. 44, pp. 19–22, 1982.
[41] H. Rajbenbach, J. P. Huignard, and Ph. Refregier, "Amplified phase-conjugate beam reflection by four-wave mixing with photorefractive $Bi_{12}SiO_{20}$ crystals," *Opt. Lett.*, vol. 9, pp. 558–560, 1984.
[42] Ph. Refregier, L. Solymar, H. Rajbenbach, and J. P. Huignard, "Two-beam coupling in photorefractive $Bi_{12}SiO_{20}$ crystals with moving grating: Theory and experiments," *J. Appl. Phys.*, vol. 58, pp. 45–57, 1985.
[43] M. Cronin-Golomb, B. Fischer, J. Nilsen, J. O. White, and A. Yariv, "Laser with dynamic holographic intracavity distortion correction capability," *Appl. Phys. Lett.*, vol. 41, pp. 219–220, 1982.
[44] B. Fischer and S. Sternklar, New optical gyroscope based on the ring passive phase conjugator," *Appl. Phys. Lett.*, vol. 47, pp. 1–3, 1985.
[45] S. K. Kwong, M. Cronin-Golomb, and A. Yariv, "Optical bistability and hysteresis with a photorefractive self-pumped phase conjugate mirror," *Appl. Phys. Lett.*, vol. 45, pp. 1016–1018, 1984.
[46] S. K. Kwong and A. Yariv, "Bistable oscillations with a self-pumped phase conjugate mirror," *Opt. Lett.*, to be published.
[47] D. Z. Anderson, "Coherent optical eigenstate memory," *Opt. Lett.*, vol. 11, pp. 56–58, 1986.
[48] B. H. Soffer, G. J. Dunning, Y. Owechko, and E. Marom, "Associative holographic memory with feedback using phase-conjugate mirrors," *Opt. Lett.*, vol. 11, pp. 118–120, 1986.
[49] A. Yariv and S. K. Kwong, "Associative memories based on message bearing optical modes in phase conjugate resonators," *Opt. Lett.*, vol. 11, pp. 186–200, 1986.
[50] J. M. Ramsy and W. B. Whitten, "Phase-conjugate feedback into a continuous-wave ring dye laser," vol. 10, pp. 362–364, 1985.
[51] There was a session on "Beam cleanup and beam combining" at the *Conf. Lasers Electroopt. CLEO'85*, Tech. Dig. WA1-5, WG1-5.
[52] A. Yariv, *Quantum Electronics*, 2nd ed. New York: Wiley, 1975, ch. 18, eq. (18.4-13).
[53] The distortion media used in these experiments were prepared by etching pieces of glass (1 mm thickness) in 48 percent HF acid for 1 min.
[54] Eq. [3.4] reduces to [1.46] in the undepleted pump approximation and reduces to [1.11] in plane wave approximation.
[55] M. Cronin-Golomb, J. Paslaski, and A. Yariv, "Vibrational resistance, short coherence length operation, and mode-locked pumping in passive phase conjugate mirrors," *Appl. Phys. Lett.*, vol. 47, pp. 1131–1133, 1985.

Sze-Keung Kwong was born in Hong Kong on August 5, 1958. He received the B.Sc. degree in physics from University of Hong Kong in 1980, the M.S. degree in physics from University of Southern California, Los Angeles, in 1981, and the Ph.D. degree in physics from the California Institute of Technology, Pasadena, in 1986.

His research interests include photorefractive effect, two-wave and four-wave mixings, phase conjugation, image processing, associative memories, bistabilities, and optical fiber sensors.

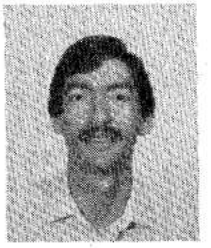

Mark Cronin-Golomb received the B.Sc. degree from the University of Sydney, Sydney, Australia, in 1979, and the Ph.D. degree in physics from the California Institute of Technology, Pasadena, in 1983.

As an undergraduate, he investigated the use of holographic diffraction gratings in enhancing the characteristics of solar selective thin film absorbers. From 1979 until 1984 he was at the California Institute of Technology working first on a neutrino scattering experiment at the Fermi National Accelerator Laboratory and then carrying out research in nonlinear optics and phase conjugation in photorefractive materials. He is currently at Ortel Corporation, Alhambra, CA, where his research interests include techniques for combining photorefractive phase conjugation with GaAlAs laser technology, and the development of photorefractive optical limiters and switches.

Ammon Yariv (S'56–M'59–F'70), for a photograph and biography, see p. 448 of the March 1986 issue of this JOURNAL.